

Initial Signatures of Magnetic Field and Energetic Particle Fluxes at Tail Reconfiguration: Explosive Growth Phase

S. OHTANI,¹ K. TAKAHASHI, L. J. ZANETTI, T. A. POTEMRA, AND R. W. MCENTIRE

Applied Physics Laboratory, The Johns Hopkins University, Laurel, Maryland

T. IJIMA

Department of Earth and Planetary Science, Faculty of Science, University of Tokyo, Tokyo, Japan

Active Magnetospheric Particle Tracer Explorers/Charge Composition Explorer (AMPTE/CCE) magnetometer and Medium Energy Particle Analyzer (MEPA) data are used to examine the initial signatures of tail field reconfiguration observed in the near-Earth magnetotail ($< 9 R_E$). Sixteen events are selected preliminarily from 9 months (January-September 1985) of magnetometer data according to two criteria, that is, an unambiguous commencement of tail field reconfiguration and a sharp recovery of the north-south (H) component. The second criterion requires that the satellite was close to the onset region of current disruption. Although these strict criteria result in the small number of events, the magnetic and particle flux signatures of the events are considered to be informative concerning the mechanism of substorm onsets. It is found that these tail reconfiguration events are classified into two types: Type I and Type II. In Type I events a current disruption starts in a flux tube that is inward (earthward/equatorward) of the spacecraft, and consequently, the spacecraft is immersed in a hot plasma region expanding from inward (earthward/equatorward). The other type (Type II) is characterized by a distinctive interval (explosive growth phase) just prior to the local commencement of tail reconfiguration. The duration of this interval is typically 1 min, much shorter than that of the so-called growth phase. During this interval the north-south magnetic (H) component is depressed sharply, and the flux of energetic ions increases outward (tailward/poleward) of the spacecraft, suggesting that the cross-tail current is explosively enhanced. It is also found that the radial magnetic (V) component changes with a distinctive phase relationship relative to the north-south component, which can also be explained in terms of the explosive enhancement in the cross-tail current intensity just prior to the current disruption. This enhancement is inferred to be a local process, rather than a result of a current disruption which has occurred somewhere else, although it is possible that the commencement of the H recovery observed is not exactly simultaneous with a substorm onset. The present results contribute significantly to modeling efforts regarding the triggering mechanism of substorms in the magnetotail.

1. INTRODUCTION

The sequence of substorms can be understood in terms of the development of the cross-tail current. The increase in the tail current intensity begins typically 1 hour before substorm onsets [Fairfield and Ness, 1970; Aubry and McPherron, 1971; see Arnoldy, 1971]. This distinctive interval is often referred to as the growth phase [e.g., McPherron, 1972]; a significant portion of the energy consumed during substorms is stored in the magnetosphere during this phase [e.g., Baker et al., 1985]. The development of the cross-tail current results in the antisunward stretching of the tail field lines [e.g., McPherron, 1972; Kokubun and McPherron, 1981] and the thinning of the plasma sheet [Hones et al., 1971, 1984; McPherron, 1972]. Substorm onsets in the magnetosphere are marked by the recovery of the tail field from this stressed configuration to a more dipolar configuration [e.g., Cummings et al., 1968; McPherron, 1972; Kokubun and McPherron, 1981], indicating that the current intensity decreases suddenly (i.e., current disruption). The disruption of the cross-tail current also results in the expansion of the plasma sheet [e.g., Hones et al., 1984]. It is well known that the tail current disruption expands both in the azimuthal [Nagai,

1982; Arnoldy and Moore, 1983] and in the radial directions [Russell and McPherron, 1973; Ohtani et al., 1988, 1992; Lopez and Lui, 1990] from a localized onset region.

Substorm-associated variations of energetic particle fluxes in the magnetotail have also been examined by many researchers [e.g., Lezniak and Winckler, 1970; Erickson and Winckler, 1973; Walker et al., 1976; Baker et al., 1978; Erickson et al., 1979; Sauvaud and Winckler, 1980; Mauk and Meng, 1986, and references therein]. Energetic particle fluxes increase rapidly at substorm onsets. This increase is usually called particle injection, although the flux increase often starts inward (earthward and/or equatorward), not outward (tailward and/or poleward), of spacecraft, which is interpreted in terms of the motion of the outer boundary of trapped particles by Walker et al. [1976]. Variations in particle fluxes are closely correlated with changes of the tail field configuration [e.g., Erickson et al., 1979; Sauvaud and Winckler, 1980].

One of the outstanding problems concerning substorms is the triggering mechanism of the current disruption. Observational determination of the location of the onset region is necessary for assessing this problem. Ohtani et al. [1992] have statistically reexamined the onset region from the viewpoint of the radial expansion of the tail current disruption and have found that the current disruption usually starts in the near-Earth magnetotail and often within $15 R_E$ from the Earth. This result is consistent with previous reports on the onset region [Hones et al., 1973; Nishida and Nagayama, 1973; Ohtani et al., 1988]. Some recent case studies have shown that the current disruption occurs initially in the near-Earth magnetotail, within $9 R_E$ from the Earth [Takahashi et al., 1987; Lui et al., 1988; Lopez et al., 1989, 1990; Ohtani et al., 1991]. Lui et al. [1992] have

¹Formerly at Department of Earth and Planetary Science, University of Tokyo, Tokyo, Japan.

Copyright 1992 by the American Geophysical Union.

examined in detail 15 current disruption events observed in the same range of radial distance and have suggested that the current disruption is triggered by the cross-field current instability [Lui *et al.*, 1991]. Kaufmann [1987] have also suggested that the tail current intensity changes most drastically at altitudes between 7 and 9 R_E during substorms. Ohtani *et al.* [1990] have reported that the region 1 and the region 2 field-aligned currents are closed with the radial current in the nightside synchronous region during substorms and suggested that a significant portion of the energy consumed during substorms is produced in this region. Thus it would be most useful to examine the tail current disruption in the near-Earth magnetotail in more detail for understanding the triggering mechanism of substorm onsets.

In this paper we examine the tail current disruption with high-time-resolution magnetic field and energetic particle data from the Charge Composition Explorer (CCE) of the Active Magnetospheric Particle Tracer Explorers (AMPTE) mission. This spacecraft has an equatorial elliptical orbit with an apogee at 8.8 R_E ; therefore its orbit is most convenient for examining the current disruption in the near-Earth tail. The primary interest in this study involves fine-scale structures observed during a short interval around the commencement of tail reconfiguration. Such structures are expected to give information on the triggering mechanism of the current disruption. The data used in this study are introduced in section 2. In section 3 we introduce briefly two types of tail reconfiguration, and then examine examples of each type in detail. In section 4 these two types of signatures are interpreted in terms of the development of the tail current; we focus our attention on the enhancement of the tail current during a short interval (explosive growth phase) just prior to the current disruption. Section 5 is the summary.

2. DATA

AMPTE/CCE has an elliptical orbit with an apogee at 8.8 R_E , a period of about 16 hours, and an orbital inclination of 4.8°. In this study we examine the tail current disruption in the near-Earth magnetotail by combining the magnetometer data and the energetic particle data obtained with the Medium Energy Particle Analyzer (MEPA). The details of these instruments are reported by Potemra *et al.* [1985] and McEntire *et al.* [1985]. We also refer to ground magnetograms obtained at 30 stations distributed in a wide range of latitude in order to specify ground substorm activities. However, it would be practically impossible to determine, from ground magnetograms, an onset time within a time resolution of 1 min; this is the typical duration of the initial magnetic disturbance during tail reconfiguration, as will be seen later. Therefore in the present study the comparison of timing between a ground substorm onset and the commencement of the tail reconfiguration observed with AMPTE/CCE should be regarded as suggestive.

The present study uses 6.2-s median and 1-s averaged vector magnetometer measurements of AMPTE/CCE. The magnetic data will be presented in VDH coordinates. In this cylindrical coordinate system, H is antiparallel to the dipole axis, V points radially outward and is parallel to the magnetic equator, and D completes a right-hand orthogonal system (positive eastward). The antisunward stretching of the tail field configuration corresponds to the increase in the absolute value of the V component ($|V|$) and/or the decrease in the H component, while the reconfiguration is marked by the decrease in $|V|$ and/or the increase in H .

The MEPA data used are the flux in the all-ion channels ECH0 through ECH4, which cover the nominal energy range of 25 keV to 285 keV; MEPA experienced an increasing gain shift with time, so the corrected energy bands are used for each event. MEPA scans the plane normal to the spin axis of the satellite which is roughly

along the Earth-Sun line, and directional fluxes are measured by dividing the spin plane into 32 angular sectors. One spin period (~6 s) is the highest possible resolution for the sectorized data. The channels cycle between the ion head and the time-of-flight (TOF) head every 96 s, with 72 s of ion head followed by 24 s of TOF data. We examine the 24-s sector-and-spin averaged flux of the five ECH channels and the anisotropy of the fluxes (32 samples) observed during a spin period.

The anisotropy of fluxes is very useful for examining the spatial inhomogeneity of the energetic particle population [e.g., Walker *et al.*, 1976]. The detector samples fluxes of particles with $\alpha \sim 90^\circ$ (α , pitch angle) twice every spin. We refer to the fluxes of particles with $75^\circ < \alpha < 105^\circ$ coming from positive and negative GSE Y direction as $J(Y+)$ and $J(Y-)$, respectively. $J(Y+)$ and $J(Y-)$ represent the flux of particles having their guiding centers inward (earthward/equatorward) and outward (tailward/poleward) of the spacecraft, respectively (see Figure 1). It should be noted that generally the detector orientation is not exactly aligned with the Y axis when it measures $J(Y+)$ and $J(Y-)$; in fact, it is possible that the looking direction deviates significantly toward the Z direction if the magnetic field has a large Y (azimuthal) component. In order to confirm that the difference between $J(Y+)$ and $J(Y-)$ actually represents the anisotropy in the Y direction, we also examine the anisotropy of fluxes measured during an individual spin period.

In the near-Earth magnetotail, the density of energetic particles decreases with the distance from the Earth, and with the distance from the neutral sheet, as well. Therefore it is expected that $J(Y-)$ is larger than $J(Y+)$ under quiet conditions. However, during substorms, the flux anisotropy should depend also on the spacecraft location relative to the acceleration region. The direction of the

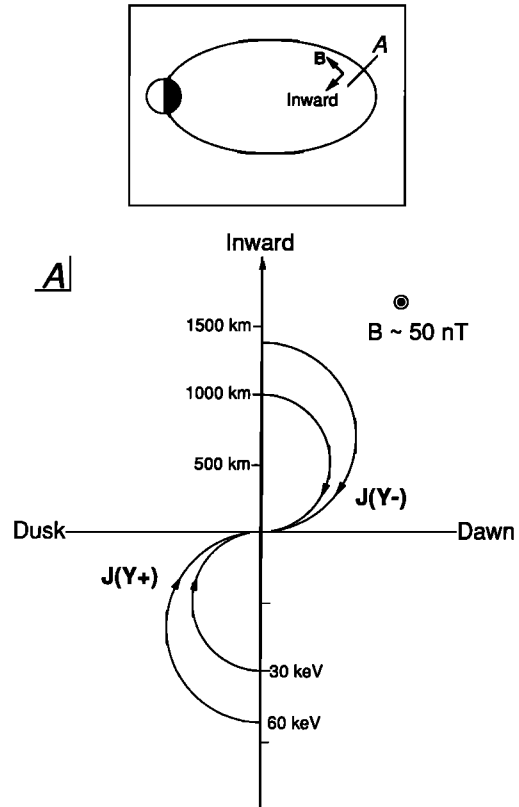


Fig. 1. Gyration orbits of protons with different energies in the plane A (see inset). Guiding centers are located tailward and/or poleward (earthward and/or equatorward) of the spacecraft when the detector is looking positive (negative) Y direction.

density gradient, which is inferred from the difference between $J(Y+)$ and $J(Y-)$, depends on the inclination of the magnetic field; if the magnetic field is northward (tailward), the difference represents the gradient in the radial (north-south) direction. Since CCE stays usually on closed field lines, our major concern is whether the flux enhancement (recovery) starts in flux tubes inward or outward of the spacecraft, rather than whether the gradient is in the radial or vertical direction.

3. OBSERVATIONS

3.1. Type I and Type II Tail Reconfiguration Events

We examine initial signatures of magnetic field and energetic particle fluxes associated with the tail reconfiguration by using the high-time-resolution data of AMPTE/CCE. We adopted two criteria for the preliminary selection of events. Since the AMPTE/CCE spacecraft stays usually in the current layer due to its small orbital inclination, it is expected that the spacecraft often observes the current disruption. On the other hand, irregular magnetic fluctuations are superimposed upon the large-scale field configuration changes in the plasma sheet, making it difficult to identify the initial signature associated with the current disruption. Therefore the first criterion is the selection of events in which the commencement of the reconfiguration can be unambiguously identified. The second criterion is that the H component must recover very sharply; the initial H increase must occur within a few minutes. If the spacecraft is located far from the onset region, it will observe the gradual changes in the magnetic field disturbance due to the time accumulation of the effects of the current disruption which is expanding in both the radial and azimuthal directions. On the other hand, if the spacecraft is located close to the onset region, most of the contribution to the reconfiguration will come from the current disruption near the spacecraft, and therefore the spacecraft should observe a sharp change in the field configuration. Hence it is expected that the initial signatures selected give information on the triggering mechanism of the current disruption. We should emphasize that we selected events irrespective of the sharpness of V signatures. In contrast to sharp H recoveries, sharp V recoveries can be caused by the rapid movement of the spacecraft relative to the current layer, and therefore does not necessarily mean the occurrence of onsets close to the spacecraft.

We surveyed the AMPTE/CCE magnetometer data during the period from January to September in 1985. During this period the spacecraft surveyed the nightside local time sector, from 1800 to 0600 in MLT; data were accumulated such that there was no evident dawn-dusk asymmetry in the local-time coverage of observations. First, we made 2-hour plots of 6.2-s median values for all the tail reconfiguration events selected from orbital plots of magnetic field data, and then selected events according to the criteria; 16 events qualified for selection. Table 1 lists the time and location of the spacecraft for each of the 16 events, as well as information on the magnetic field prior to the commencement of the tail reconfiguration.

By expanding signatures observed during the several minutes around each onset of tail reconfiguration, we found that the 16 events that were selected can be classified into two groups: Type I and Type II. The sequence of changes in the H and the V components, as well as the particle flux variation, observed in each type of tail reconfiguration are schematically illustrated in Figure 2. In Type I events, the magnitude of the V component begins to decrease before H increases, followed by irregular variations, while Type II events are characterized by a transient depression of the H component just prior to recovery. The energetic particle population starts to increase inward of the spacecraft in Type I events and outward of the spacecraft in Type II events, suggesting that the difference in magnetic signatures arises from the difference in the spacecraft position relative to the current disruption region or flux tube. The relative timing between the magnetic field and energetic particle signatures is generally different from case to case. (The only exception is the increase in $J(Y+)$ in Type II events, which starts prior to the commencement of the H recovery.) This would be so because the changes in the magnetic field components can be observed even if the spacecraft is distant from the region of current disruption, while enhancements in energetic particle fluxes cannot be observed unless the spacecraft is located within one Larmor radius of the energization region or the boundary of an energetic particle regime. Note that flux enhancements can be observed also in association with the motion of the boundary of trapped particles [e.g., Walker *et al.*, 1976].

For some of the selected events the MEPA data are not available, or the flux anisotropy cannot be confirmed because of small fluxes or inconvenient geometry between the magnetic field and the

TABLE 1. List of the Events

Type	Day	UT	R	MLT	MLat	Z	$ \Theta $	H	V
2	116	2131	6.9	0.3	-8.5	-0.2	20.1 (23.7)	22.9 (36.7)	62.5 (83.6)
1	119	1452	8.6	1.1	-13.0	-0.6	6.7 (23.7)	6.2 (18.7)	52.9 (42.7)
1	134	1455	8.6	0.3	-14.4	-0.7	6.2 (21.8)	5.1 (16.8)	46.8 (41.9)
2	135	2206	8.6	0.4	-7.0	0.4	32.7 (31.0)	13.9 (19.0)	21.6 (31.6)
2	143	0136	8.3	23.8	3.7	1.2	37.1 (46.3)	24.5 (28.3)	-32.4 (-27.1)
2	150	0747	8.8	23.7	3.0	1.1	43.3 (49.1)	25.2 (24.5)	-26.8 (-21.2)
2	150	1004	8.4	0.4	-0.6	0.8	63.7 (70.7)	30.7 (30.3)	-15.2 (-10.6)
2	151	1531	8.8	23.9	-15.2	-0.7	9.8 (6.0)	4.4 (4.2)	25.5 (40.0)
2	152	2122	8.6	23.8	-6.8	0.6	22.8 (63.1)	5.8 (21.1)	13.8 (10.7)
1	154	2239	8.7	0.3	-4.5	0.5	20.6 (78.3)	2.8 (23.7)	7.4 (4.9)
1	158	2209	8.1	0.6	-6.4	0.4	58.4 (26.8)	10.1 (17.0)	6.2 (33.7)
2	164	1528	8.8	22.8	-15.7	-0.5	19.0 (18.9)	12.4 (15.5)	36.0 (45.0)
2	180	0657	8.7	21.9	0.9	1.0	52.0 (54.5)	29.3 (26.3)	-22.9 (-18.8)
2	211	0420	6.7	22.4	9.0	1.3	40.2 (37.4)	60.3 (56.6)	-71.4 (-74.2)
2	226	0328	7.5	21.2	8.6	1.3	31.3 (35.4)	38.7 (39.4)	-63.6 (-55.4)
1	257	1241	5.6	20.8	-10.7	-0.8	18.2 (47.7)	44.4 (119.9)	135.4 (109.0)

Locations (radial distance, magnetic local time, magnetic latitude, the distance from the magnetic equator estimated according to Lopez [1990]), and the magnetic inclination, H , and V averaged over 1 min centered at 3 min before the commencement of the H recovery; numbers in the parentheses are estimates from the Tsyganenko [1989] model.

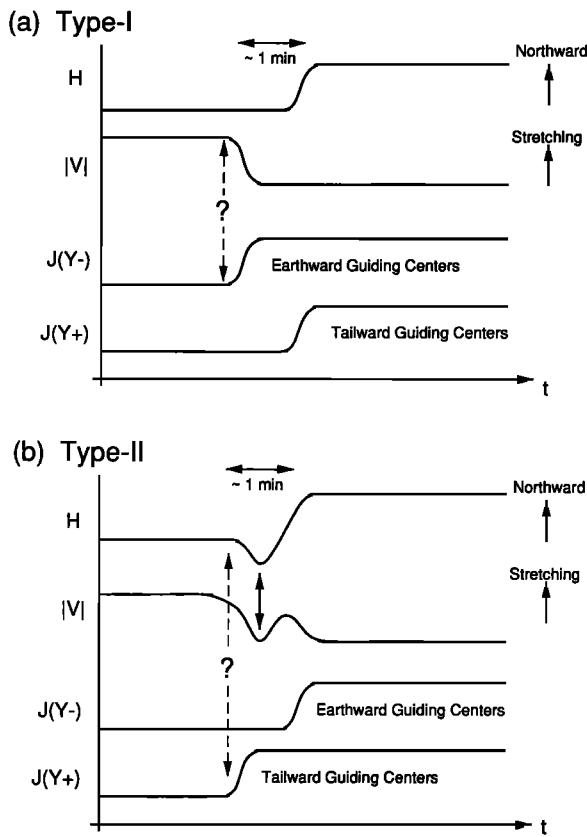


Fig. 2. Schematic illustration of changes in H , V , $J(Y-)$, and $J(Y+)$ in (a) Type I and (b) Type II tail reconfiguration.

satellite spin axis. Consequently, we use only the magnetometer data for classifying tail reconfiguration events. However, we should emphasize that we could not find any events in which the anisotropy of the energetic ion fluxes contradicts our classification. We classified the 16 events into Type I and Type II events by examining higher-resolution (1-s) data. We found 5 Type I events and 11 Type II events.

The small number of events, 16 in total, is probably due to our restrictive selection procedure. As mentioned at the beginning of this section, the selection of events with sharp recoveries of the H component suggests that the spacecraft was very close to the initial location of the current disruption. Our previous case study [Ohtani *et al.*, 1991], which examined one of the Type II events (day 211 event), has shown that the spatial scale of the onset region is $\sim 1 R_E$ or less in both the radial and azimuthal directions. On the other hand, during the 9-month period, CCE surveyed the nightside near-Earth tail at $r < 8.8 R_E$ without any preference for local time. If onsets of the current disruption occur at random at $6.6 R_E < r < 10 R_E$ and $18 < LT < 06$, the chance of the spacecraft encounter of the onset region is given as $(\pi \times 0.5 R_E \times 0.5 R_E) / (0.5 \times \pi \times 10 R_E \times 10 R_E - 0.5 \times \pi \times 6.6 R_E \times 6.6 R_E) \sim 0.01$. Let us assume that substorms occur at a rate of five per day. Hence the total number of substorms which are expected to occur during 9 months is estimated to be $5 \times 30 \times 9 = 1350$, and therefore the number of Type I and Type II events expected to be observed during the same interval is estimated to be $1350 \times 0.01 \sim 14$. The result is not much different from the number of events which we selected. Although the occurrence distribution of substorm onsets is not as simple as assumed above, we believe that the selected events reveal general properties of the commencement of the (local) current disruption.

3.2. April 29, 1985 Event: An Example of the Type I Tail Reconfiguration

In this subsection we show an example of the Type I tail reconfiguration (Figure 2a). The event we examine took place at about 1452 UT on April 29, 1985. The spacecraft was located at $8.6 R_E$ from the Earth in the postmidnight magnetotail. Figure 3 presents the magnetic field and energetic particle data during the event. The particle data are sector-and-spin averaged over four spins (~ 24 s), and the magnetic field data are 6.2-s median values. The H component suddenly increased at ~ 1452 UT, and the V component began to decrease slightly before the H increase (this time delay can be easily identified in the expanded plot, Figure 4); that is, the magnetic configuration changed to a more dipolar one. It should also be noted that the particle fluxes increased without any evident energy dispersion. On the ground, a positive bay onset was observed at ~ 1451 UT at Kakioka (207.9° geomagnetic longitude, 25.6° geomagnetic latitude) and Memambetsu (210.4° , 34.6°). The AE index also revealed the commencement of a small substorm ($AE \sim 250$ nT). Therefore, the change of the tail configuration observed at AMPTE/CCE was associated with this substorm onset.

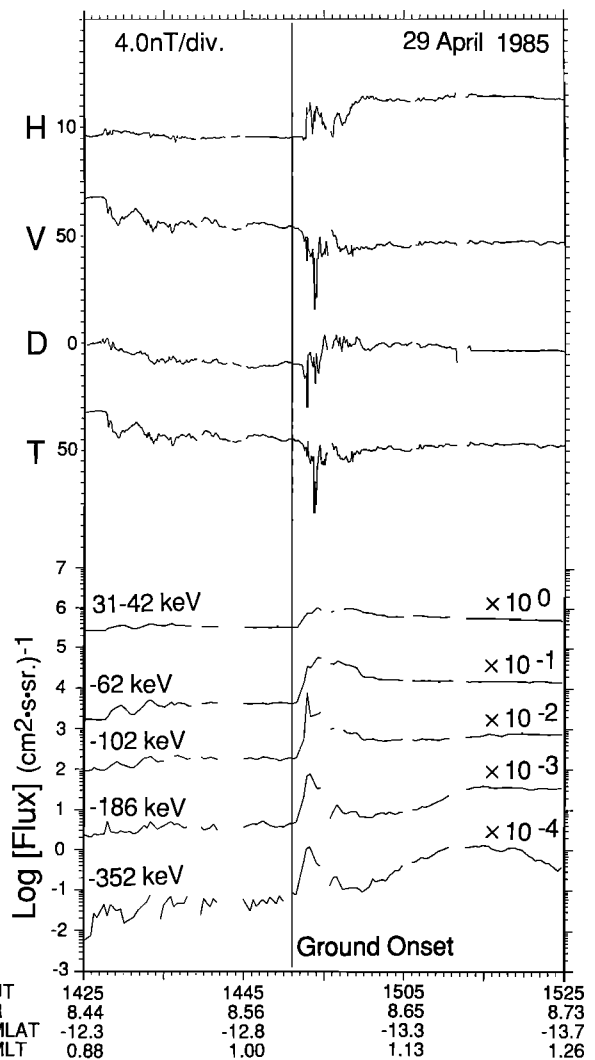


Fig. 3. Magnetic field and energetic proton measurements from AMPTE/CCE for a tail reconfiguration event on April 29, 1985. The magnetic field data are 6.2-s median values, and the particle data are spin averaged over 24 s. The spacecraft locations (R: radial distance; MLAT: magnetic latitude; MLT: magnetic local time) are indicated at the bottom. The ground substorm onset at 1451 UT is marked by the vertical line.

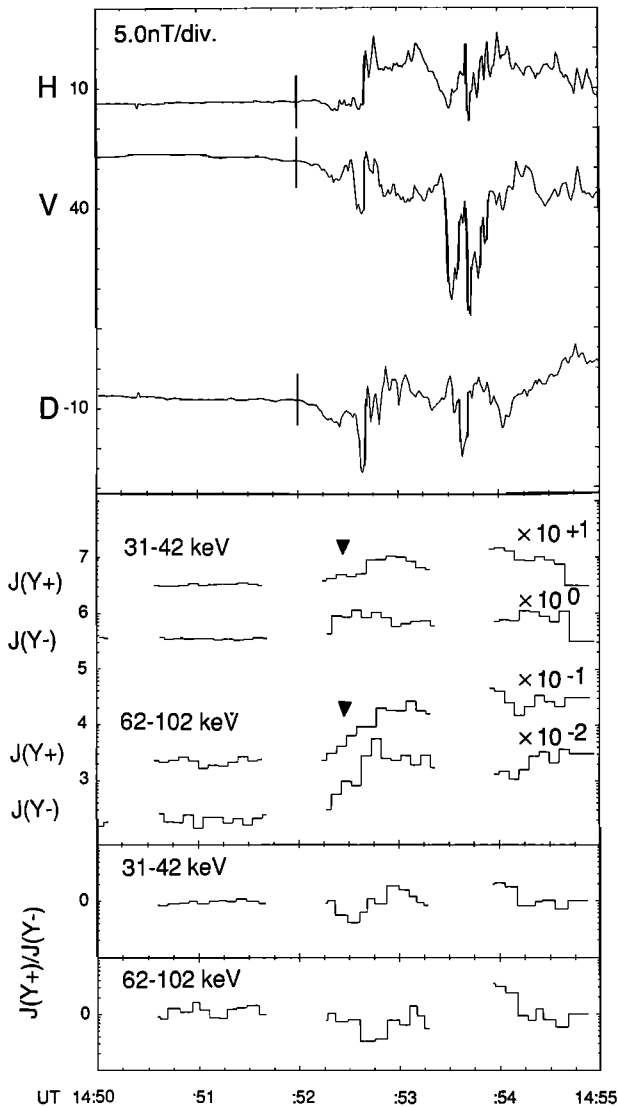


Fig. 4. High time resolution measurements of the magnetic field and the energetic proton fluxes of the two MEPA channels during the period around the commencement of the tail reconfiguration of the April 29 event, 1450–1455 UT. The particle data are plotted separately with respect to the sign of the GSE Y direction of the detector; $J(Y+)$ and $J(Y-)$ represent fluxes coming from the positive and negative Y directions, respectively. The ratio between $J(Y+)$ and $J(Y-)$ is plotted in the bottom panel.

The tail reconfiguration is presented in detail in Figure 4, which shows the 1-s magnetic field data and the sectored MEPA data from the two channels having the highest time resolution, 31–42 and 62–102 keV; the periodic appearance of gaps in the $J(Y+)$ and $J(Y-)$ plots is due to the cycle of the MEPA operation mentioned in section 2. The H component suddenly increased at 1452:40 UT. V began to decrease at 1452:00 UT, about 40 s before this H increase. The commencement of the negative D deviation was almost simultaneous with the V decrease; D was transiently depressed, followed by the steplike increase (also see Figure 3). It should also be noted that the magnitudes of fluctuations were enhanced in all the magnetic components after 1452:00 UT. Thus we conclude that the decrease in V was the earliest magnetic signature observed in association with the tail reconfiguration.

The particle fluxes also changed in correlation with the magnetic signatures. In the lower-energy channel, $J(Y-)$ began to increase at 1452:20 UT, during the period of the initial V decrease,

while no obvious change in $J(Y+)$ can be found until 1452:40 UT. In the higher-energy channel, $J(Y-)$ began to increase at \sim 1452:20 UT more sharply than $J(Y+)$, although the time difference between the two is not as evident as that found in the lower-energy channel (see also $J(Y+)/J(Y-)$ in the bottom panels). Figure 5 shows the flux anisotropy during the spin period of 1452:25–1452:31 UT; this period was embedded between the commencement of the V decrease and that of the H increase and is marked by the inverted triangles in Figure 4. The flux of each angular sector is presented as a function of pitch angle. The “+” (“-”) signs represent the flux measured when the detector orientation has a positive (negative) Y component. At a given pitch angle the flux was higher when the detector looked in the negative Y direction. The anisotropy in the higher-energy channel, which is not as evident as that in the lower-energy channel, may be due to the lower count rate of the higher-energy channel. We conclude that the difference between $J(Y+)$ and $J(Y-)$ is actually due to the anisotropy in the Y direction. Hence we infer that the hot-plasma region expanded outward

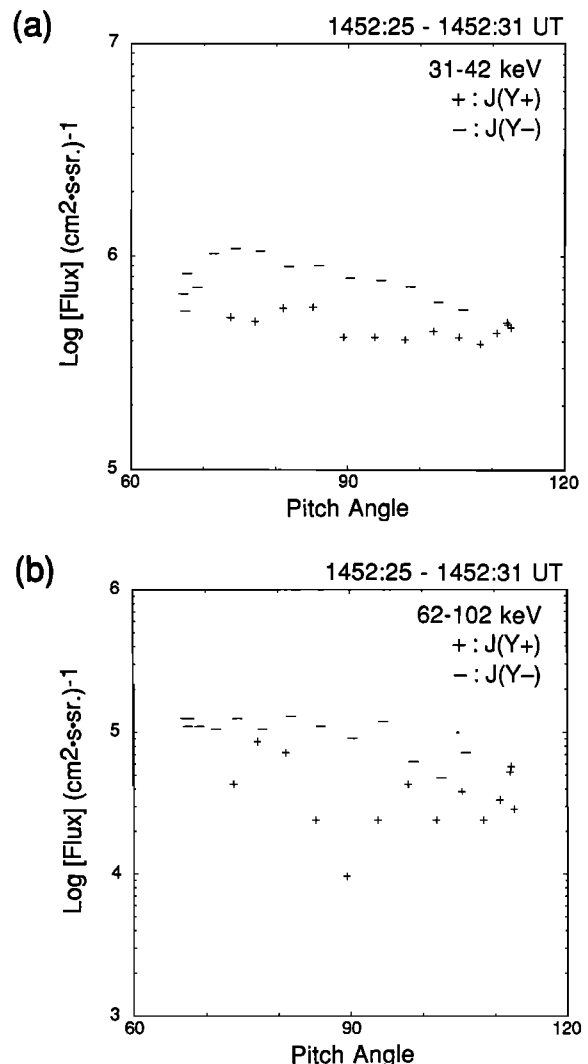


Fig. 5. The flux anisotropy during the one spin period from 1452:25–1452:31 UT, which is marked by the inverted triangles in Figure 4. The fluxes of each angular sector are presented as a function of pitch angle. The “+” (“-”) signs represent the flux measured when the detector orientation has a positive (negative) Y component; here measurements with detector orientation at large angles from the Y direction ($|\cos \Theta_Y| < 0.2$; Θ_Y : an angle between the detector orientation and the GSE Y axis) are excluded from the figure. The coverage of pitch angles is limited due to the two-dimensional scan of the MEPA detector.

(tailward/poleward) from inward (earthward/equatorward) of the spacecraft position and that the spacecraft was immersed in the hot plasma in the course of this expansion.

In closing, the characteristics of the Type I tail reconfiguration is summarized as follows (see also Figure 2a). (1) In the course of the tail reconfiguration, first, $|V|$ starts to decrease, and then H increases suddenly with a significant time delay. (2) The flux of energetic ions starts to increase inward of the spacecraft.

3.3. June 29, 1985 Event: An Example of the Type II Tail Reconfiguration

An example of the Type II tail reconfiguration (Figure 2b) is shown in Figure 6. The spacecraft was located at $8.7 R_E$ from the Earth in the premidnight (~ 21.9 MLT) magnetotail. In this event, H and V increased almost simultaneously at 0657 UT. At that time, a negative bay onset was observed at Yellowknife (298.4° geomagnetic longitude, 69.6° geomagnetic latitude). In accordance with the very sharp decrease in the X (north-south) magnetic component at Yellow Knife, the AE index suddenly increased by ~ 300 nT, suggesting that a certain activity started at that time. At AMPTE/CCE, ion fluxes also changed in association with the tail reconfiguration. The flux in the lowest-energy (34–46 keV) channel decreased, while the fluxes in the other channels increased without

any evident energy dispersion. The flux enhancement accompanying a decrease in low-energy particle fluxes was also reported by Moore et al. [1981]; they interpreted such energy dependence in terms of the heating of plasma sheet plasma [see Arnoldy, 1986].

Figure 7 shows this event with higher-time-resolution data in the same format as Figure 4. The absolute value of the V component ($|V|$) began to increase at 0656:20 UT, and H began to decrease almost simultaneously. The depression of the H component just prior to the tail reconfiguration is the most characteristic signature of the Type II tail reconfiguration. The commencement of the H increase coincided with that of the transient negative V deviation; the correlation of variations between H and V will also be examined for other events in section 3.4.

The MEPA data show that the flux of energetic ions started to change outward of the spacecraft more than 1 min before the recovery of the magnetic field configuration. In the lower-energy (34–46 keV) channel, which observed the decrease in flux at the onset of the tail reconfiguration (see Figure 6), $J(Y+)$ began to decrease

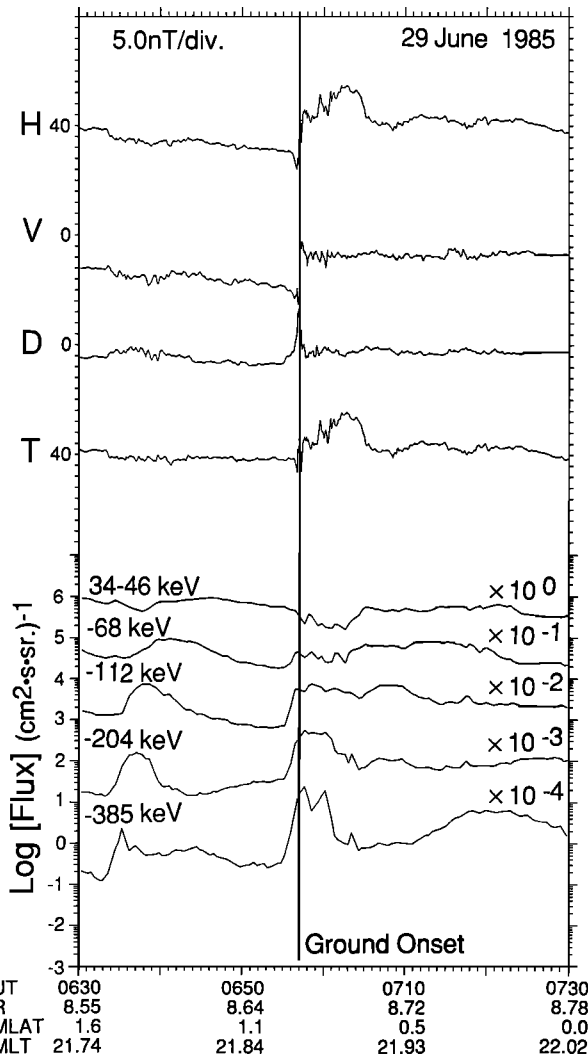


Fig. 6. Magnetic field and energetic proton measurements from AMPTE/CCE for a tail reconfiguration event on June 29, 1985, shown in the same format as Figure 3.

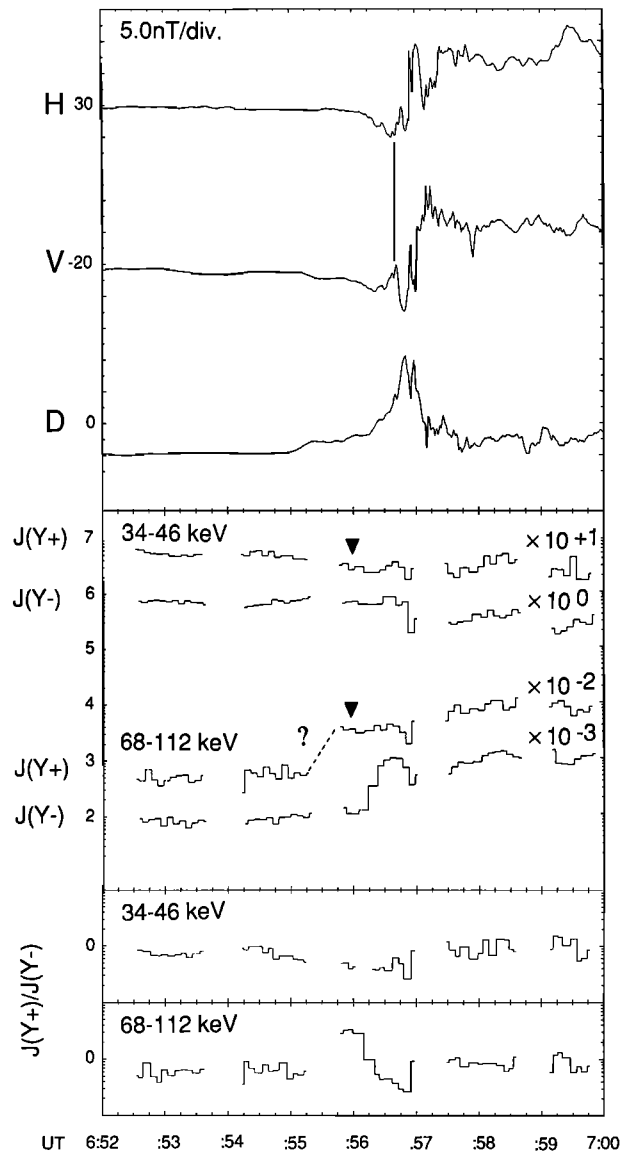


Fig. 7. High time resolution measurements of the magnetic field and the energetic proton fluxes of the two MEPA channels during the period around the commencement of the tail reconfiguration of the June 29 event, 0652–0700 Ut, shown in the same format as Figure 4.

gradually around at 0655 UT, whereas $J(Y-)$ was almost constant until it decreased suddenly at 0656:50 UT. In the higher-energy (68–112 keV) channel, $J(Y+)$ increased almost by an order between 0655:20 and 0655:45 UT; the timing cannot be determined exactly because of the unfortunate data gap (see section 2). On the other hand, $J(Y-)$ in the higher-energy range increased suddenly at 0656:15 UT with a significant time delay (at least 30 s) from the increase in $J(Y+)$. The order of commencement of changes in $J(Y+)$ and $J(Y-)$ was just the opposite of that of the April 29, 1985, event (Figure 4). It should also be noted that $J(Y+)$ was significantly larger than $J(Y-)$ during the 30-s interval (see the ratio of $J(Y+)$ and $J(Y-)$ shown at the bottom of Figure 7). That is, the anisotropy was just the opposite of that expected for a steady magnetotail (section 2).

Figure 8 shows the anisotropy of fluxes during 0655:56–0656:02 UT in the same format as Figure 5; $J(Y+)$ began to change before this period, but $J(Y-)$ did not (the period is marked by the inverted triangles in Figure 7). In the lower-energy channel, the fluxes of particles coming from the negative Y direction are significantly larger than that of particles coming from the positive Y direction irrespective of pitch angles. In the higher-energy range, the anisotropy was just the opposite during the period, and became the same as that found in the lower-energy channel after the increase in $J(Y-)$

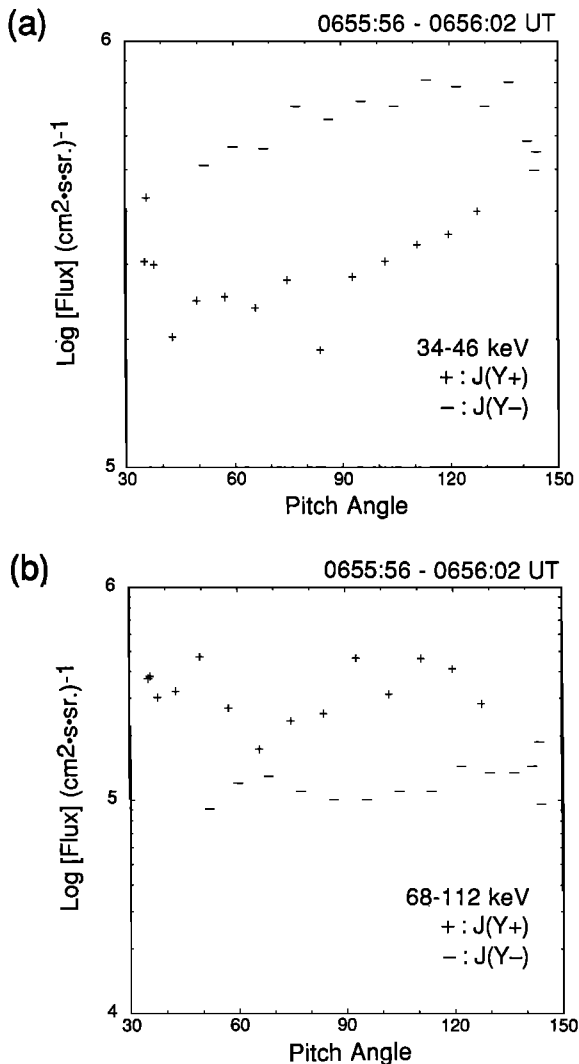


Fig. 8. The flux anisotropy during the one spin period from 0655:56–0656:02 UT, which is marked by the horizontal bars in Figure 7, shown in the same format as Figure 5.

at 0656:15 UT (not shown). These particle signatures suggest that the energization started outward (tailward/poleward) of the spacecraft, and that the spacecraft was immersed in the hot plasma region in association with the tail reconfiguration.

In summary, the Type II tail reconfiguration is characterized by a distinctive interval just prior to the commencement of the tail reconfiguration (also see Figure 2b). The duration of this interval is much shorter than that of the conventional growth phase. During this interval the north-south magnetic component is depressed sharply, and the energetic particle population increases outward of the spacecraft.

3.4. Timing of the H and V Changes in Type II Events

The most distinctive signature of the Type II tail reconfiguration is the transient depression of the H component just prior to the sharp recovery. Type II tail reconfiguration is often observed with AMPTE/CCE. Figure 9 shows three other events, in which a spike-like depression of the H component prior to the tail reconfiguration is very evident. The top panels are 30-min plots of the magnetometer data, and the bottom panels show the commencement of the tail reconfiguration in more detail by expanding 5 min around the initial

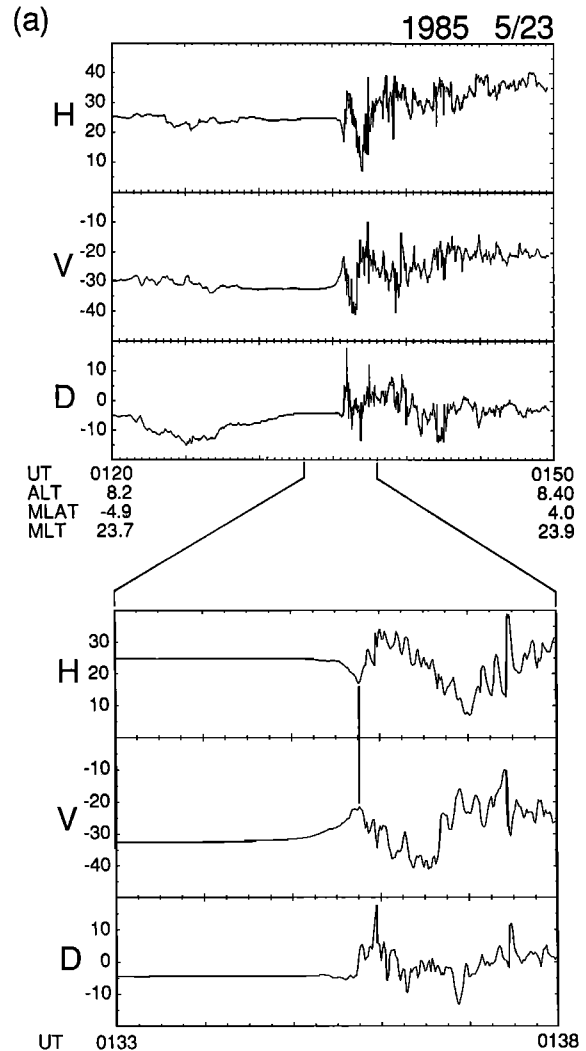


Fig. 9. Magnetic field data from three Type II tail reconfiguration events on (a) May 23, 1985, (b) May 30, 1985, and (c) June 13, 1985. For each event, the top panel is a 30-min plot, and the bottom panel expands a 5-min period centered at the initial sharp increase in H . The spacecraft locations are indicated at the bottom of the top panels.

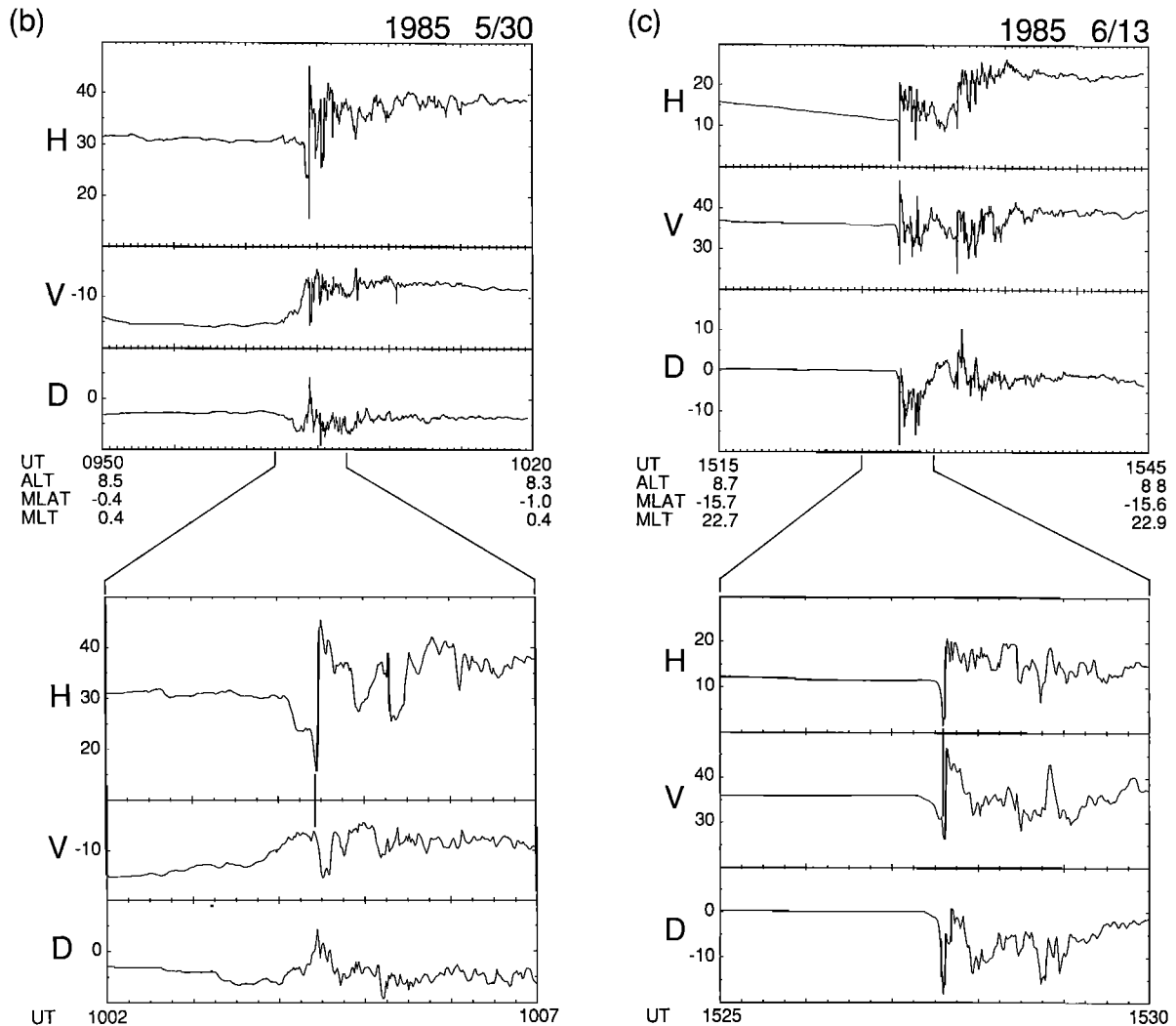


Fig. 9. (continued)

sharp recovery of H . H and $|V|$ tended to increase and decrease, respectively, during the events (see the 30-min plots), as expected from the tail reconfiguration from a stressed configuration to a more dipolar one. The AE index started to increase almost simultaneously with the H recovery, suggesting that the observed tail reconfiguration was caused by the tail current disruption.

The start of the H increase is marked by the vertical lines in the high-time-resolution plots. As can be found easily, $|V|$ decreases during the period of the H depression, and the commencement of the increase in H coincided with that of the increase in $|V|$. The H increase and the $|V|$ increase occurred simultaneously in the 1-s data. Such correlation can also be found in the June 29 event (Figure 7); see also Figure 4 of Ohtani *et al.* [1991]. The same correlation was found between the H and V components for each of the 11 Type II events selected. This finding is very useful for interpreting this type of tail reconfiguration, as will be discussed.

3.5. Spatial Distribution of Type I and Type II Events

Figure 10 represents the equatorial distribution of Type I and Type II events, which are represented by the open and solid circles, respectively. The difference in distribution is not evident between the two types. (Although four of the five Type I events were ob-

served in the postmidnight region, the number of events is not large enough to be conclusive.) As will be discussed in the next section, the two types of the tail reconfiguration signatures do not necessarily mean two different mechanisms of current disruption, but they would simply reflect the difference of the spacecraft position relative to the initial disruption region. Since the energetic particle population starts to change inward (earthward/equatorward) of CCE in Type I events, and outward (tailward/poleward) in Type II events, it would be expected that Type I events are observed at higher latitudes and/or at larger radial distances than Type II events. However, we could not find any evident difference in radial distance and in magnetic latitude of the occurrence between the Type I and the Type II events (see Table 1); this may be due to the small number of the Type I events. On the other hand, the smaller occurrence of Type I events suggests that the tail current disruption starts more frequently outside of the CCE orbital coverage. The overall occurrence of both types of events is significantly skewed toward the premidnight sector. The sharp recovery of H , which is the criterion for the event selection, can be ascribed to the sudden disruption of the tail current near the spacecraft, as discussed in section 3.1. Therefore the skewed distribution suggests that the onsets of the current disruption tend to occur more frequently in the premidnight sector.

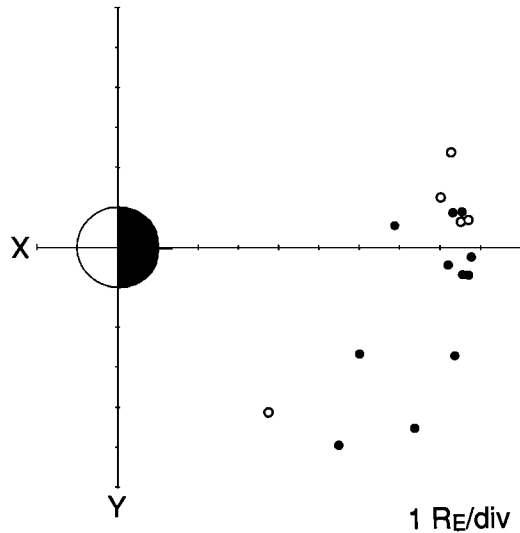


Fig. 10. The distribution of Type I and Type II tail reconfiguration events, projected on the equatorial plane. The open and solid circles represent the Type I and Type II events, respectively.

4. DISCUSSION

4.1. Interpretation

In the previous section we examined the initial signatures of the tail reconfiguration with a time resolution on the order of seconds, and found that the signatures can be classified into two types: Type I and Type II. Since the H component increased suddenly in both of the two types, it is unlikely that the signatures are simply spatial structures observed when the spacecraft crossed field lines along which distant effects have propagated. It is therefore reasonable to discuss these two types in terms of the local change in a current system near the CCE spacecraft.

4.1.1. Type I events. In Type I events, $|V|$ initially starts to decrease, followed by an increase in H , as observed in the April 29 event (section 3.1). The flux of energetic ions increases in a flux tube inward (earthward/equatorward) of the spacecraft position in association with the $|V|$ decrease, indicating that the tail current intensity changes also inward of the spacecraft position. Since the spacecraft observes a decrease in $|V|$, the change in the current intensity can be regarded as resulting from the current disruption. Here the flux tube associated with this current change may cross the neutral sheet further tailward of the spacecraft. The current disruption results in the plasma sheet expansion, and consequently the spacecraft observes the enhancement in the flux of energetic ions coming from inward of the spacecraft position ($J(Y-)$). The decrease in $|V|$ could also be caused by the immersion of the spacecraft in the expanding current sheet. Walker *et al.* [1976] have reported that in some cases energetic particle fluxes start to increase, first on guiding centers earthward/equatorward of spacecraft at substorm onsets. They interpreted this spatial gradient in terms of the motion of the outer boundary of trapped particles. Lopez *et al.* [1989] have found that the particle injection is composed of an earthward streaming edge, followed by a relatively isotropic plasma region, for tail reconfiguration events in which the magnetic field strength decreases; note that the magnetic strength decreased in the course of the tail reconfiguration also in the April 29 event (see Figure 3). Lopez *et al.* have argued that the plasma sheet expands from equatorward of the spacecraft in association with the tail current disruption. These previous findings are consistent with the result of this study.

The time sequence of the D deviation observed in Type I events also favors the above interpretation. In the April 29 event the transient D depression began almost simultaneously with the decrease in $|V|$, followed by the steplike increase (see Figure 3). The reversal of the sign of the D deviation could be ascribed to the motion of a field-aligned current sheet relative to the spacecraft; that is, the field-aligned current was generated in association with the tail current disruption inward of the spacecraft position, and then passed over the spacecraft in the course of the poleward expansion of the plasma sheet. The D deviation reveals such a reversal of sign in four of the five Type I events we selected, while the deviation was very irregular in the other event.

On the other hand, we infer from the increase in H that at that time the current is disrupted on the tailward side of the spacecraft. The time delay of the H increase from the $|V|$ decrease suggests that the disruption region expands tailward; therefore it is quite possible that a substorm onset takes place before the commencement of the H recovery. It should also be noted that the spacecraft was within the plasma sheet (or plasma sheet boundary layer) before the tail reconfiguration in the April 29 event, as suggested by the particle fluxes at almost same levels as those after the reconfiguration (see the lowest-energy channel of the MEPA data in Figure 3). Taking into account that the current disruption starts in the flux tube inward of the spacecraft in Type I events, we conclude that onsets of the current disruption often take place within the near-Earth plasma sheet.

4.1.2. Type II events. The other type (Type II) of the tail reconfiguration is characterized by a distinctive interval just prior to the sharp increase in H . The duration of this interval is typically 1 min, much shorter than the so-called growth phase. During this interval the H magnetic component is depressed sharply, and the flux of energetic ions starts to increase first in a flux tube outward of the spacecraft. Therefore we should discuss the H depression in terms of the change in the current intensity that is occurring in a flux tube outward of the spacecraft. We infer from Biot-Savart's law that the tail current intensity is enhanced explosively during this period of H depression. The increase in $J(Y+)$ observed before the tail reconfiguration at the spacecraft position may be responsible for this current enhancement. The sharp recovery of H , which follows the depression, is regarded as the commencement of the tail reconfiguration, in the conventional sense, and can be ascribed to tail current disruption which also occurs outward of the spacecraft, presumably in the same flux tube in which the current intensity has been enhanced explosively. The explosive enhancement of the tail current intensity, followed by the disruption, may be a fundamental process of the substorm triggering mechanism.

We found in section 3.4 that in Type II events the commencement of the H recovery coincides with the commencement of the $|V|$ increase, which is preceded by the transient decrease. This coincidence of the timing between the H and $|V|$ changes is also explained in terms of the present scenario, as schematically shown in Figure 11. Since the spacecraft is in the near-Earth magnetotail, we expect that changes in the current intensity take place along a flux tube, rather than in a region localized around the equator. Note that $|V|$ does not depend on the hemisphere of the spacecraft location, although the spacecraft is in the northern hemisphere in the figure. We also assume that the tail current intensity changes primarily in the shaded flux tube which surrounds the spacecraft as shown in the figure. Since our present concern is the sign of the H and V changes, we assume an equinoctial geometry of the flux tube in Figure 11. Quantitative studies, for example, on amplitudes of the H and $|V|$ changes need more assumptions on the distribution of the current density, including the seasonal variation of the plasma sheet con-

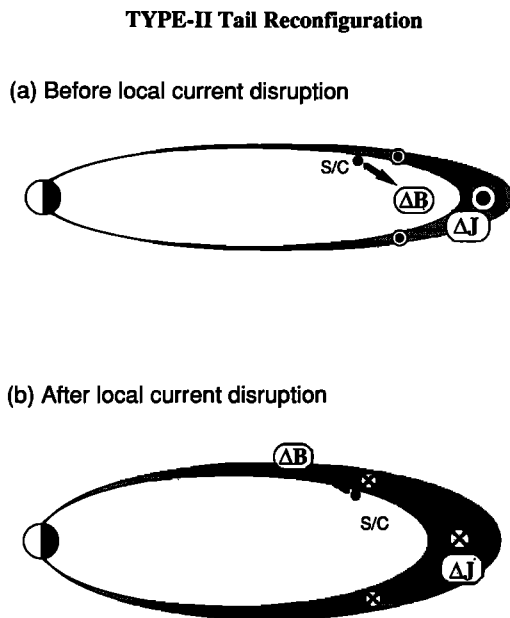


Fig. 11. Illustration of a possible interpretation of the Type II event. The shaded area represents the flux tube in which the tail current intensity changes drastically in the course of the tail reconfiguration. It is assumed that the tail current intensity increases transiently (Figure 11a), and then decreases suddenly (Figure 11b) in this flux tube.

figuration and the spatial size of the flux tube, which would make the discussion speculative. Hence we would like to make a qualitative discussion, as follows.

Magnetic deviations of different magnetic components result from the change in the current intensity at different parts of the flux tube. That is, the change in the current intensity tailward of the spacecraft causes magnetic deviations in the H magnetic component, while the change poleward of the spacecraft causes magnetic deviations primarily in the V component. As discussed previously, we infer that the current intensity is enhanced in the flux tube suddenly before the current disruption. The current enhancement near the equator of the flux tube results in the decrease in H , while the current enhancement in the poleward part of the flux tube results in the decrease in $|V|$ (Figure 11a). The enhancement in the current intensity is followed by the current disruption, which is equivalent to the reversal of the direction of the deviation current. Therefore the sign of deviations in each of the magnetic components should be reversed at the commencement of the current disruption. That is, both H and $|V|$ decrease (Figure 11b). Thus the coincidence between the commencement of the H recovery and the increase in $|V|$, which is observed in Type II events, is explained by assuming that the tail current is enhanced explosively before the current disruption in a flux tube surrounding the spacecraft.

There are, at least, two effects which are in general important in interpreting magnetic field and particle flux changes, but are not relevant to the Type II events; that is, effects of field-aligned currents and those of injected plasma. First, one may try to explain the H and $|V|$ signatures observed in Type II events in terms of the field-aligned currents of the substorm current wedge, which forms in association with current disruption. Figure 12 shows the difference in H and $|V|$ signatures between the observation and the prediction from the current wedge model. In usual tail field configurations magnetic fields have both northward and earthward (tailward) components in the northern (southern) hemisphere. Consequently, outside the current wedge the magnetic deviation caused by the

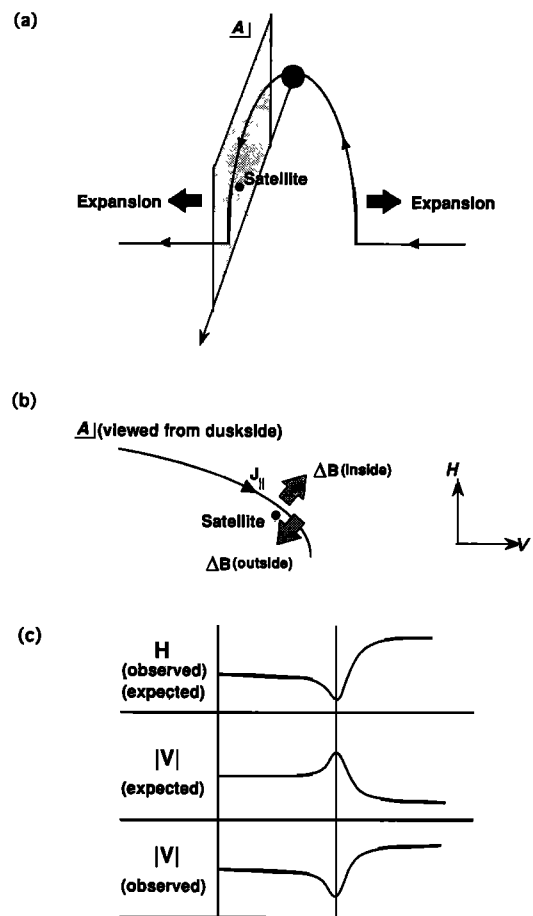


Fig. 12. The difference in H and $|V|$ signatures between the observation and the prediction from the current wedge model. (a) The azimuthal expansion of the current wedge. (b) Magnetic deviations caused by the wedge currents in the meridional plane (A). (c) Magnetic signatures expected from the azimuthal expansion of the wedge current, compared with observations of Type II events.

wedge currents has a negative H component and a negative (positive) V component in the northern (southern) hemisphere (Figure 12b); note that this does not depend on whether the satellite is on the duskside or dawnside of the current wedge. Inside the current wedge the sign of the magnetic deviation is reversed in each component. Thus H decreases and $|V|$ increases outside the current wedge, and H increases and $|V|$ decreases inside the current wedge. The H depression followed by a sharp H recovery may be caused by a wedge field-aligned current passing the spacecraft azimuthally in the course of the azimuthal expansion of the current wedge (Figure 12a). In such a case for the current wedge model we expect that $|V|$ increases and then decreases in correlation to the H deviation (Figure 12c). However, the opposite $|V|$ deviation is observed in Type II events.

Moreover, if the H depression of the Type II tail reconfiguration is a result of the current disruption which took place somewhere at a different local time, the observed enhancement in the ion fluxes would imply the arrival of ions drifting azimuthally. However, for such a case, there is no reason why the spacecraft would observe the flux anisotropy as shown in Figure 8, as well as the significant time delay between the increases in $J(Y+)$ and $J(Y-)$. Thus we conclude that the H and $|V|$ deviations we examined are caused primarily by changes in the tail current intensity.

One may also try to explain the transient depression of the H

component (and the total field strength) in the Type II tail reconfiguration in terms of the diamagnetic effect of the injected plasma. This interpretation is based on the assumption that the tail current disruption takes place before the local H depression, since the injection results from the enhancement in the dawn-to-dusk electric field due to the current disruption. In this case the spacecraft is expected to observe first the compressional wave (fast magnetosonic wave), which would cause the increase in H , propagating earthward from the onset region [Moore *et al.*, 1981; see Russell and McPherron, 1973], and then to observe the diamagnetic signatures when the injected plasma reaches the spacecraft. However, such a precursory signature was not observed in the Type II events (see sections 3.2 and 3.3), suggesting that the diamagnetic effect cannot account for the H depression.

On the other hand, it is possible that the local explosive enhancement in the tail current intensity shields the effects of the current disruption which may have occurred a little more tailward before the sharp H recovery. In such a case a substorm onset would occur before the H recovery at AMPTE/CCE. We should emphasize again that it is practically impossible to determine, from ground magnetograms, a substorm onset time within a time resolution of 1 min. However, the enhancement in $J(Y+)$ associated with the H depression and the correlation between H and $|V|$ signatures indicate that the explosive enhancement in the tail current intensity is a local process associated with the current disruption, rather than a result of a current disruption which has occurred somewhere else. Therefore with regard to the local development of the tail current intensity, we would not have to distinguish the onset of substorms from the onset of the local current disruption.

4.1.3. Other points. The presence of the two different types of the tail reconfiguration signatures does not necessarily mean two mechanisms of the tail current disruption, but it would simply reflect the difference of the spacecraft position relative to the onset flux tube. That is, the spacecraft is located poleward of the onset flux tube in Type I events, while the spacecraft is surrounded by the onset flux tube in Type II events. The comparison of the field inclination before the tail reconfiguration (see Table 1) would support this claim. It seems that the spacecraft is located on more Sun-Earth directed field lines in Type I events than in Type II events, except for the day 158 event. It should also be noted that the observed inclination is significantly smaller, that is, more Sun-Earth aligned, than the field model prediction in Type I events (also except for the day 158 event), while the difference is not so large, less than 10° , in Type II events, except for one event (the day 152 event). These facts suggest that the spacecraft is located poleward of the current enhancement region in Type I events, while the spacecraft is located inward (or inside) of the current enhancement region in Type II events. This is consistent with our interpretation of each of the two types of tail reconfiguration.

It would be reasonable to expect, for Type I events, that the spacecraft should observe the explosive enhancement in the tail current intensity before the current disruption. The expected magnetic signature would be the sudden increase in $|V|$. However, in all the five Type I events selected in this analysis, $|V|$ tended to decrease continuously, at least until the commencement of the H recovery, and such an increase in $|V|$ could not be found. Multisatellite observations would be necessary for testing our interpretation of the two types of tail reconfiguration, which will be the subject of future studies.

4.2. Explosive Growth Phase

The explosive enhancement in the tail current intensity during a short interval just prior to the current disruption is one of the most

important findings of this study. The duration of this distinctive interval is typically 1 min, much shorter than that of the conventional growth phase; hence the interval may be referred to as the explosive growth phase. Figure 13 schematically shows the development of the tail current intensity in the onset region during substorms. As discussed in the previous section, the explosive enhancement in the tail current intensity is a local process, rather than a result of a current disruption which has occurred somewhere else. Therefore the present discussion would also be applicable outside the onset region, if the current disruption is triggered locally (section 4.1.2). During the growth phase the current intensity continues to increase gradually, resulting in the increase in the lobe field magnitude, and also resulting in the thinning of the plasma sheet. Then the intensity begins to increase explosively, and accordingly, the plasma sheet becomes thinner. Finally, the plasma sheet becomes unstable to a certain instability, which triggers the current disruption; that is, a substorm onset takes place.

The enhancement in the tail current intensity and the behaviors of plasma sheet ions could be explained in terms of a positive feedback between the current intensity and the number of nonadiabatic (unmagnetized) ions. The motion of ions becomes nonadiabatic when the thickness of the plasma sheet becomes comparable to the Larmor radius [Büchner and Zelenyi, 1989]. As the intensity of the tail current increases, the plasma sheet becomes thinner, and consequently more ions become nonadiabatic and contribute further to the tail current. Moreover, the thinning of the plasma sheet corresponds to the enhancement in the gradient of the field strength and the field line curvature, which would result in the increase in the duskward velocity of ion drifts.

McPherron *et al.* [1987] have inferred that the scale height of the plasma sheet thinned to ~ 400 km at $X \sim -13 R_E$ before a local current disruption in the March 22, 1979, event (Coordinated Data Analysis Workshop (CDAW) 6 event) [see Ohtani *et al.*, 1988]. This scale height is comparable to the Larmor radius of ions with an energy of ~ 3 keV for a magnetic field strength of 20 nT, indicating that nonadiabatic behavior of ions is important in considering the structure of the current sheet. Recently, Mitchell *et al.* [1990] examined the carriers of the tail current in the course of tail reconfiguration and found that the enhancement of the cross-tail current just prior to the local current disruption is carried by nonadiabatic ions. A similar feedback mechanism is also possible for the curvature drift of particles [Pellinen and Heikkilä, 1984; Kaufmann, 1987]. The energization of ions could be ascribed to the increase in the mobility of ions in the dawn-to-dusk direction; the drift is in the same direction as the large-scale electric field, and therefore ions gain energy as they drift duskward. Unmagnetized

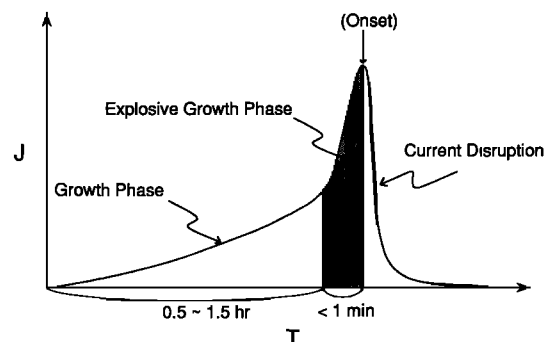


Fig. 13. Schematic illustration of the change in the tail current intensity in the course of substorms. The current intensity continues to increase gradually in the growth phase, then increases explosively in the explosive growth phase, followed by a sudden disruption.

ions would drive an instability which trigger substorms. The cross-field current instability recently proposed by *Lui et al.* [1991] is a possible candidate for the triggering instability.

The energy range of MEPA channels used is 25 keV to 285 keV or higher, which is higher than the typical ion temperature in the near-Earth plasma sheet, which is ~ 10 keV [Moore et al., 1987; Lui, 1992]. One of our interests is whether ions observed with MEPA can be the carriers of the tail current. With regard to the adiabatic drifts of ions, namely, the gradient B drift and the curvature drift, the drift velocity is proportional to the energy of particles. By assuming a Maxwellian distribution with a temperature of 10 keV, the contribution of ions above 30 keV to the total energy density is estimated at $\sim 20\%$. If the characteristic length of the spatial gradient of the particle density does not depend on particles' energy, the magnetization current is also proportional to the energy density. Therefore the contribution of ions above 30 keV to the total current (the diamagnetic current) is $\sim 20\%$. However, higher-energy ions have a larger Larmor radius and can become nonadiabatic more easily. Therefore we suggest that they contribute to the current density more significantly.

The localization of the substorm onset region could also be understood in terms of the present scenario of the tail current development during substorms. It is well known that the substorm onset region is localized both in the azimuthal and the radial directions; the spatial scale of the region would be of the order of $\sim 1 R_E$ or less [Ohtani et al., 1991]. On the other hand, the tail current is enhanced in much larger region in the near-Earth magnetotail before substorm onsets. In fact, the current disruption expands both in the radial and the azimuthal directions, suggesting that the energy has been stored also outside of the onset region during the growth phase. Here one of the most important problems is why substorm onsets take place in a localized region despite the rather homogeneous enhancement in the tail current intensity. Figure 14 schematically shows the change in the tail current intensity during a substorm at two locations; let us assume that one point (A) is in the onset region and the other point (B) is outside of, but very close to, the onset region. During the growth phase the tail current intensity increases continuously both at A and B; hence we assume that the intensity in the onset region (A) is slightly larger than that outside of the onset region (B). Therefore the thickness of the plasma sheet becomes comparable to the ion's Larmor radius first at A, and consequently, the current intensity begins to increase explosively there. When the plasma sheet is locally so distorted that it becomes

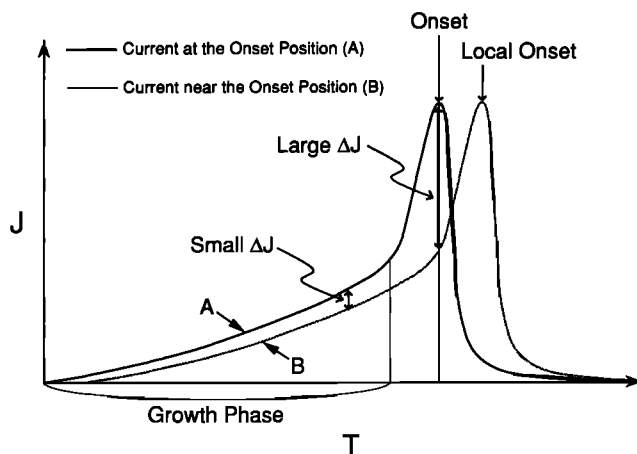


Fig. 14. Schematic illustration of the change in the tail current intensity in the onset region (A) and outside of the onset region (B). It is assumed that the current intensity is slightly larger at A than at B during the growth phase, and that the explosive growth phase begins first at A.

unstable to a certain instability, the tail current is disrupted and a substorm commences. On the other hand, the current intensity outside of the onset region (B) is still increasing gradually when the explosive growth phase starts at A, and the plasma sheet is still stable to the instability at B. Note that during this interval there is a significant difference in the current intensity between the two locations. Consequently, the current disruption would start in a localized region.

In the above discussion we assumed that there is a slight difference in the tail current intensity between inside and outside of the onset region during the growth phase. However, the present model would be still applicable, even if the current intensity develops homogeneously, but the ion's Larmor radius, which depends on the ion's energy and the magnetic strength, is not homogeneous in the near-Earth magnetotail. In such a case, the explosive development of the tail current would start first in the region where the Larmor radius is largest, and consequently the substorm onset takes place there. This may be one reason why the distribution of the Type II events is significantly skewed toward dusk (see section 3.4); note that the average energy of ions is higher in the premidnight sector than in the postmidnight sector [Hardy et al., 1989].

Distinctive intervals just prior to substorm onsets have also been pointed out from different viewpoints. *Pellinen and Heikkila* [1984] examined a sequence of auroral luminosity during a substorm, and found that an auroral arc fades about 1 or 2 min before an auroral breakup [see *Pellinen and Heikkila*, 1978]. They also discussed a configuration of the tail current in terms of a current sheet pinch. *Baker and McPherron* [1990] also suggested a similar current system and discussed it in terms of the near-Earth neutral line formation. Modeling of a three-dimensional current system, including ionospheric currents, is a crucial problem of the triggering process of tail current disruption. We think that our results place important constraints on such modeling.

5. SUMMARY

We have examined the initial signatures of tail reconfiguration in detail with the AMPTE/CCE magnetic field and MEPA data. From the 9-month (January–September 1985) magnetometer data we selected 16 events which satisfy two criteria, that is, the unambiguous identification of the commencement of tail field reconfiguration and the sharp recovery of the north-south component. The unexpectedly small number of events selected, despite the long-term data we surveyed, is probably due to the second criterion, which requires that the satellite was close to the onset region of the current disruption. We found that these tail reconfiguration events are classified into two types. One type (denoted as Type I) is ascribed to a tail current disruption which starts in a flux tube inward (earthward and/or equatorward) of the spacecraft location. In this case the absolute value of the V component ($|V|$) begins to decrease first, followed by an increase in the H component. Energetic particle fluxes also increase in flux tubes inward of the spacecraft location in association with the $|V|$ decrease, indicating that the hot plasma region expands from within the spacecraft location. The other type of tail reconfiguration (Type II) is characterized by a distinctive interval (explosive growth phase) just prior to the commencement of tail reconfiguration; the duration of this interval is typically 1 min, much shorter than that of the growth phase. The H component is depressed sharply during the explosive growth phase. The particle flux anisotropy indicates that the particle energization begins in a flux tube outward (tailward/poleward) of the spacecraft location, suggesting that the H depression is caused by the explosive enhancement in the tail current intensity, which also takes place outward of the spacecraft location. The coincidence of timing be-

tween H and V signature around the commencement of the Type-II tail reconfiguration can also be explained in terms of the explosive enhancement in the cross tail current intensity preceding the current disruption. This enhancement is inferred to be a local process, rather than a result of a current disruption which has occurred somewhere else. The present results would place important constraints on modeling the triggering of tail current disruption.

Acknowledgments. The authors wish to thank R. E. Lopez, A. T. Y. Lui, B. H. Mauk, T. Tamao, and V. A. Sergeev for helpful conversations. Work at APL was supported by NASA and NSF. Correlative aspects of this work at the University of Tokyo were supported by the Japanese Society for the Promotion of Science for Japanese Junior Scientists under grant 01790262. Ground-based magnetograms were provided through World Data Center C2 for Aurora, National Institute of Polar Research. The program for the *Tsyganenko* [1989] model was provided by N. A. Tsyganenko to R. L. McPherron, and subsequently modified by R. Nakamura.

The editor would like to thank R. Pellinen, R. L. McPherron and one other referee for their assistance in evaluating this paper.

REFERENCES

- Arnoldy, R. L., Signature in the interplanetary medium for substorms, *J. Geophys. Res.*, **76**, 5189, 1971.
- Arnoldy, R. L., Fine structure and pitch angle dependence of synchronous orbit electron injections, *J. Geophys. Res.*, **91**, 13411, 1986.
- Arnoldy, R. L., and T. E. Moore, Longitudinal structure of substorm injections at synchronous orbit, *J. Geophys. Res.*, **88**, 6213, 1983.
- Aubry, M. P., and R. L. McPherron, Magnetotail changes in relation to the solar wind magnetic field and magnetospheric substorm, *J. Geophys. Res.*, **76**, 4381, 1971.
- Baker, D. N., and R. L. McPherron, Extreme energetic particle decreases near geostationary orbit: A manifestation of current diversion within the inner plasma sheet, *J. Geophys. Res.*, **95**, 6591, 1990.
- Baker, D. N., P. R. Higbie, E. W. Hones, Jr., and R. D. Belian, High-resolution energetic particle measurements at $6.6 R_e$, 3, Low-energy electron anisotropies and short-term substorm predictions, *J. Geophys. Res.*, **83**, 4863, 1978.
- Baker, D. N., T. A. Fritz, R. L. McPherron, D. H. Fairfield, Y. Kamide, and W. Baumjohann, Magnetotail energy storage and release during the CDAW 6 substorm analysis intervals, *J. Geophys. Res.*, **90**, 1205, 1985.
- Büchner, J., and L. M. Zelenyi, Regular and chaotic charged particle motion in magnetotail-like field reversals, 1, Basic theory of trapped motion, *J. Geophys. Res.*, **94**, 11821, 1989.
- Cummings, W. D., J. N. Barfield, and P. J. Coleman, Jr., Magnetospheric substorms observed at the synchronous orbit, *J. Geophys. Res.*, **73**, 6887, 1968.
- Erickson, K. N., and J. R. Winckler, Auroral electrojets and evening sector electron dropouts at synchronous orbit, *J. Geophys. Res.*, **78**, 8373, 1973.
- Erickson, K. N., R. L. Swanson, R. J. Walker, and J. R. Winckler, A study of magnetosphere dynamics during auroral electrojet events by observations of energetic electron intensity changes at synchronous orbit, *J. Geophys. Res.*, **84**, 931, 1979.
- Fairfield, D. H., A statistical determination of the shape and position of the geomagnetic neutral sheet, *J. Geophys. Res.*, **85**, 775, 1980.
- Hardy, D. A., M. S. Gussenhoven, and D. Brautigam, A statistical model of auroral ion precipitation, *J. Geophys. Res.*, **94**, 370, 1989.
- Hones, E. W., Jr., S.-I. Akasofu, S. J. Bame, and S. Singer, Poleward expansion of the auroral oval and associated phenomena in the magnetotail during auroral substorms, 2, *J. Geophys. Res.*, **76**, 8241, 1971.
- Hones, E. W., J. R. Asbridge, S. J. Bame, and S. Singer, Substorm variations of the magnetotail plasma sheet from $X_{SM} = -6 R_e$ to $X_{SM} = -60 R_e$, *J. Geophys. Res.*, **78**, 109, 1973.
- Hones, E. W., Jr., T. Pytte, and H. I. West, Jr., Associations of geomagnetic activity with plasma sheet thinning and expansion: A statistical study, *J. Geophys. Res.*, **89**, 5471, 1984.
- Kaufmann, R. L., Substorm currents: Growth phase and onset, *J. Geophys. Res.*, **92**, 7471, 1987.
- Kokubun, S., and R. L. McPherron, Substorm signatures at synchronous altitude, *J. Geophys. Res.*, **86**, 11265, 1981.
- Lezniak, T. W., and J. R. Winckler, Experimental study of magnetospheric motions and the acceleration of energetic electrons during substorms, *J. Geophys. Res.*, **75**, 7075, 1970.
- Lopez, R. E., The position of the magnetotail neutral sheet in the near-Earth region, *Geophys. Res. Lett.*, **17**, 1617, 1990.
- Lopez, R. E., and A. T. Y. Lui, A multisatellite case study of the expansion of a substorm current wedge in the near-Earth magnetotail, *J. Geophys. Res.*, **95**, 8009, 1990.
- Lopez, R. E., A. T. Y. Lui, D. G. Sibeck, K. Takahashi, R. W. McEntire, L. J. Zanetti, and S. M. Krimigis, On the relationship between the energetic particle flux morphology and the change in the magnetic field magnitude during substorms, *J. Geophys. Res.*, **94**, 17105, 1989.
- Lopez, R. E., H. Lühr, B. J. Anderson, P. T. Newell, and R. W. McEntire, Multipoint observations of a small substorm, *J. Geophys. Res.*, **95**, 18897, 1990.
- Lui, A. T. Y., Radial profiles of quiet time magnetospheric parameters, *J. Geophys. Res.*, in press, 1992.
- Lui, A. T. Y., R. E. Lopez, S. M. Krimigis, R. W. McEntire, L. J. Zanetti, and T. A. Potemra, A case study of magnetotail current sheet disruption and diversion, *Geophys. Res. Lett.*, **15**, 721, 1988.
- Lui, A. T. Y., C.-L. Chang, A. Mankofsky, H.-K. Wong, and D. Winske, A cross-field current instability for substorm expansions, *J. Geophys. Res.*, **96**, 11389, 1991.
- Lui, A. T. Y., R. E. Lopez, B. J. Anderson, K. Takahashi, L. J. Zanetti, R. W. McEntire, T. A. Potemra, D. M. Klumpar, E. M. Greene, and R. Strangeway, Current disruptions in the near-Earth neutral sheet region, *J. Geophys. Res.*, **97**, 1461, 1992.
- Mauk, B. H., and C.-I. Meng, Macroscopic ion acceleration associated with the formation of the ring current in the Earth's magnetosphere, in *Ion Acceleration in the Magnetosphere and Ionosphere*, *Geophys. Monog. Ser.*, vol. 38, edited by T. S. Chang, pp. 351-361, AGU, Washington, D.C., 1986.
- McEntire, R. W., E. P. Keath, D. E. Fort, A. T. Y. Lui, and S. M. Krimigis, The medium-energy particle analyzer (MEPA) on the AMPTE/CCE spacecraft, *IEEE Trans. Geosci. Remote Sens.*, **GE-23**(3), 230, 1985.
- McPherron, R. L., Substorm related changes in the geomagnetic tail: The growth phase, *Planet. Space Sci.*, **20**, 1521, 1972.
- McPherron, R. L., C. T. Russell, and M. P. Aubry, Satellite studies of magnetospheric substorms on August 15, 1968, 9, Phenomenological model for substorms, *J. Geophys. Res.*, **78**, 3131, 1973.
- McPherron, R. L., A. Nishida, and C. T. Russell, Is near-Earth current sheet thinning the cause of auroral substorm onset?, paper presented at Conference on quantitative modeling of magnetosphere-ionosphere coupling processes, sponsor, Kyoto Sangyo Univ., Kyoto, Japan, March 9-13, 1987.
- Mitchell, D. G., D. J. Williams, C. Y. Huang, L. A. Frank, and C. T. Russell, Current carriers in the near-Earth cross-tail current sheet during substorm growth phase, *Geophys. Res. Lett.*, **17**, 583, 1990.
- Moore, T. E., R. L. Arnoldy, J. Feynman, D. A. Hardy, Propagating substorm injection fronts, *J. Geophys. Res.*, **86**, 6713, 1981.
- Nagai, T., Observed magnetic substorm signatures at synchronous altitude, *J. Geophys. Res.*, **87**, 4405, 1982.
- Nishida, A., and N. Nagayama, Synoptic survey for the neutral line in the magnetotail during the substorm expansion phase, *J. Geophys. Res.*, **78**, 3782, 1973.
- Ohtani, S., S. Kokubun, R. C. Elphic, and C. T. Russell, Field-aligned current signatures in the near-tail region, 1, ISEE observations in the plasma sheet boundary layer, *J. Geophys. Res.*, **93**, 9709, 1988.
- Ohtani, S., S. Kokubun, R. Nakamura, R. C. Elphic, C. T. Russell, and D. N. Baker, Field-aligned current signatures in the near-tail region, 2, Coupling between the region 1 and the region 2 systems, *J. Geophys. Res.*, **95**, 18913, 1990.
- Ohtani, S., K. Takahashi, L. J. Zanetti, T. A. Potemra, R. W. McEntire, and T. Iijima, Tail current disruption in the geosynchronous region, in *Magnetospheric Substorms*, *Geophys. Monogr. Ser.*, vol 64, edited by J. R. Kan, T. A. Potemra, S. Kokubun, and T. Iijima, pp. 131-137, AGU, Washington, D. C., 1991.
- Ohtani, S., S. Kokubun, and C. T. Russell, Radial expansion of the tail current disruption during substorms: A new approach to the substorm onset region, *J. Geophys. Res.*, **97**, 3129, 1992.
- Pellinen, R. J., and W. J. Heikkilä, Observations of auroral fading before breakup, *J. Geophys. Res.*, **83**, 4207, 1978.
- Pellinen, R. J., and W. J. Heikkilä, Inductive electric fields in the magnetotail and their relation to auroral and substorm phenomena, *Space Sci. Rev.*, **37**, 1, 1984.
- Potemra, T. A., L. J. Zanetti, and M. H. Acuna, The AMPTE/CCE magnetic field experiment, *IEEE Trans. Geosci. Remote Sens.*, **GE-23**(3), 246, 1985.

- Russell, C. T., and R. L. McPherron, The magnetotail and substorms, *Space Sci. Rev.*, *15*, 205, 1973.
- Sauvaud, J.-A., and J. R. Winckler, Dynamics of plasma, energetic particles, and fields near synchronous orbit in the nighttime sector during magnetospheric substorms, *J. Geophys. Res.*, *85*, 2043, 1980.
- Takahashi, K., L. J. Zanetti, R. E. Lopez, R. W. McEntire, T. A. Potemra, and K. Yumoto, Disruption of the magnetotail current sheet observed by AMPTE CCE, *Geophys. Res. Lett.*, *14*, 1019, 1987.
- Tsyganenko, N. A., A magnetospheric magnetic field model with a warped tail current sheet, *Planet. Space Sci.*, *37*, 5, 1989.
- Walker, R. J., K. N. Erickson, R. L. Swanson, and J. R. Winckler, Substorm-associated particle boundary motion at synchronous orbit, *J. Geophys. Res.*, *81*, 5541, 1976.
-
- T. Iijima, Department of Earth and Planetary Science, Faculty of Science, University of Tokyo, Tokyo 113, Japan.
- R. W. McEntire, S. Ohtani, T. A. Potemra, K. Takahashi, and L. J. Zanetti, Applied Physics Laboratory, The Johns Hopkins University, Johns Hopkins Road, Laurel, MD 20723.

(Received April 12, 1991;
revised July 31, 1991;
accepted July 13, 1992.)